High-speed material characterization using an instrumented forging hammer

Julen Agirre[1, a)], David Abedul[1, b)], Angel Oruna[1, c)], Nagore Otegi[1, d)] and Lander Galdos[1, e)]

[1]Advanced Material Forming Processes research group, Mondragon Unibertsitatea, Loramendi 4, 20500 Arrasate-Mondragon, Spain

[a)] Corresponding author: jagirreb@mondragon.edu
[b)] dabedul@mondragon.edu
[c)] aoruna@mondragon.edu
[d)] notegi@mondragon.edu
[e)] lgaldos@mondragon.edu

Abstract. Hammer forging is a widely employed manufacturing process to produce parts with excellent mechanical properties. Although the rheological behavior and the microstructural transformation phenomena of metals under hammer forging conditions are of great industrial interest, few materials have been tested in such intermediate strain rates (10 s^{-1} to 10^3 s^{-1}) due to the lack of laboratory machines for intermediate-speed testing. With the objective of addressing that gap, this paper presents a novel automatic forging simulator comprised of an instrumented forging hammer capable of performing intermediate speed deformations, up to 5 m/s. Three data acquisition approaches were evaluated to select the most appropriate to obtain valid rheological data from intermediate strain rate tests performed on the developed hammer. First, data obtained by both a high-speed camera and a load cell was combined to calculate reference flow curves. Then, two additional data monitoring approaches were then analyzed, employing independently first the high-speed camera and then the load cell data. It was concluded that flow curves obtained utilizing only the load cell data offered accurate results without the need for an expensive and complex high-speed camera.

Keywords: Forging; Material characterization; High-speed testing; Hammer; Monitoring

1. Introduction

Hammer forging is a widely employed technology that produces parts with superior mechanical properties and with minimum material waste. The initial billet, which usually has a simple geometry, is plastically deformed in one or more operations to produce parts with complex final geometries. The process is attractive from an economic standpoint when a large number of parts must be produced and/or when superior mechanical properties are required [1]. Frequently, such exceptional mechanical properties are achievable only by a hammer forging process.

The most significant characteristic of hammer forging is the high deformation speed, and thus the high strain rates reached when forming the material. Although in other manufacturing processes such as machining operations the material is subjected to higher strain rates (10^3 s^{-1} to 10^6 s^{-1}) than those reached in hammer forging operations (10 s^{-1} to 10^3 s^{-1}), deformation speeds in hammer forging are much higher than those of press forging [2]. In the case of mechanical presses this variable can reach a maximum of only 30 s^{-1}, and no more than 10 s^{-1} in hydraulic presses [2,3].

Although the rheological behavior and the microstructural transformation phenomena of metals under hammer forging conditions are of great industrial interest, few studies have been carried out, and few materials have been tested in such intermediate strain rates. One of the main reasons is that there are not many commercial experimental facilities that allow testing under such conditions [2]. Conventional servo-hydraulic testing machines are commonly utilized for quasi-static strain rate testing ($\leq$10 s^{-1}), and high strain rate tests (>10^3 s^{-1}) are generally performed in Split Hopkinson Pressure Bar (SHPB) testing machines [2]. However, there is a lack of laboratory testing facilities to perform tests in the gap between quasi-static and high strain rates. Numerous researchers have developed testing machines for intermediate strain rate testing, such as servo-hydraulic machines or modified SHPB systems. However, excessive acquisition noise or limited achievable strain levels are the main drawbacks of these machines [2]. Furthermore, very few of these testing facilities are equipped with a heating system, resulting in a lack of machines capable of performing tests at both intermediate strain rates and high temperatures.

This paper presents a novel automatic forging simulator developed to address this gap. This laboratory-scale testing machine is able to reproduce a wide range of real cold and hot industrial forging conditions,

from low strain rates in an isothermal hydraulic press up to intermediate strain rates in an instrumented forging hammer. Additional forging strategies can also be tested, including intermediate heating cycles and combined strain rate deformations. Moreover, by modifying the sample geometry and the tooling of the forming modules, several loading conditions, such as compression, tension or shear, can also be tested.

As regards the instrumented forging hammer, data acquisition in the intermediate to high-speed range is crucial to obtain valid and representative results. There exist a number of high acquisition-rate techniques to measure the kinematics and load in these speed ranges. For kinematic data acquisition, non-contact measurement techniques are often used, e.g., high-speed cameras with Digital Image Correlation (DIC), laser displacement sensors, or customized extensometers. The load applied to the specimen is typically measured by a Hopkinson bar or by a piezoelectric load cell connected to an amplifier and an oscilloscope [2]. The instrumented hammer presented in this paper is equipped with two of the aforementioned acquisition devices: a high-speed camera with DIC, and a piezoelectric load cell with an amplifier and an oscilloscope. These two techniques were selected as they offer a good compromise between cost, versatility and robustness.

In the present paper three acquisition approaches are evaluated so as to select the most appropriate to obtain valid rheological data from intermediate strain rate tests performed on the instrumented forging hammer. For this purpose, the instrumented hammer was employed to perform cold uniaxial upsetting tests at four intermediate strain rates. The uniaxial compression test is a widely known method to determine the flow stress of a metallic material as a function of the strain applied, by compressing a cylindrical sample between two flat dies [4]. In this case, the tested material was S235JR structural steel.

First of all, data obtained by both the high-speed camera and the load cell was combined to calculate reference flow curves. With the aim of simplifying the data acquisition setup of the instrumented hammer, two additional data monitoring methods were then analyzed. These were data acquired solely by the high-speed camera to analytically calculate the flow curves, and data acquired by only the load cell to calculate the same stress-strain curves.

The suitability of each monitoring technique was evaluated in terms of the correctness and the sharpness of the acquired rheological data as well as the simplicity of the monitoring setup. Results of the three acquisition approaches were compared and evaluated and the most appropriate acquisition technique for the novel instrumented forging hammer was selected. This work forms the basis for future studies in intermediate strain rate testing, not only for flow data acquisition at these underexplored strain rates, but also for the study of microstructural transformation phenomena of metallic materials at these strain rates and under cold to hot conditions.

2. Experimental procedure

2.1. Instrumented forging hammer

Very few commercial laboratory machines are capable of testing materials at hammer forging strain rates (up to 300 s^{-1}). To address that lack, a novel automatic forging simulator was developed and constructed (Fig. 1). This automatic forging simulator was designed to perform compression, tension and shear tests, in addition to crash tests. It is comprised of four main sections: a heating furnace (max. 1350 ºC), an isothermal hydraulic press, an instrumented hammer and a quenching medium. To minimize human error and optimize manipulation times, the machine is fully automated, and sample manipulation is carried out by an electro-pneumatic system.

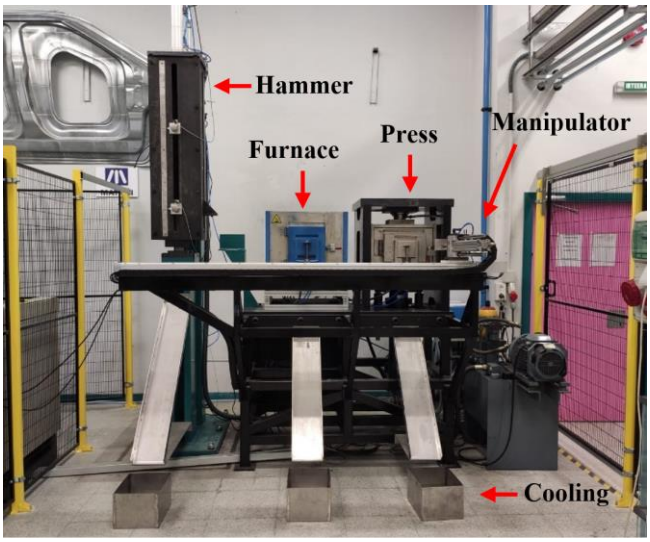

Fig. 1. Overview of the developed experimental forging simulator.

In the present paper we focus on the instrumented hammer, as it was the only deformation module employed in the study. The hammer is pneumatically actuated and capable of performing high-speed deformations, up to 5 m/s. Such elevated speeds mean that upsetting tests at strain rates of up to 300 s^{-1} can be carried out (depending on the geometry of the tested sample), thus covering the range of strain rates commonly reached in industrial hammer processes. In a conventional uniaxial upsetting test, the strain rate at which the sample is deformed is calculated by the following equation (Eq. 1):

$$\dot{\varepsilon} = \frac{v}{h} \tag{1}$$

where v and h are the instantaneous deformation velocity and instantaneous sample height, respectively. As an example, if a strain rate of 300 s^{-1} is sought in a conventional uniaxial upsetting test with an initial deformation velocity of 5 m/s, an initial sample height of 16,67 mm would be needed. If a constant strain rate is required during the straining, a decreasing deformation velocity would need to be applied to the sample.

In the instrumented forging hammer presented in this paper, the sample is deformed by kinetic energy, propelling the upper die downward with a high-pressure pneumatic cylinder. Speed variation is accomplished by modifying the falling height of the upper die, the greater the falling height, the higher the deformation velocity, and thus, the higher the deformation energy. The weight of the upper die is 92 kg, and hence the maximum applicable deformation energy is 1,15 kJ.

2.2. Uniaxial upsetting tests and data acquisition setup

With the objective of selecting the most appropriate acquisition approach to generate valid flow data at elevated strain rates, cold uniaxial compression tests were performed with the instrumented hammer at four different speeds (3,3 m/s, 4 m/s, 4,7 m/s and 5 m/s) which correspond to four different strain rates (150 s^{-1}, 200 s^{-1}, 235 s^{-1} and 260 s^{-1}, respectively). Cylindrical samples (Ø13,5x20 mm) of S235JR structural steel were employed for the tests.

Although correct lubrication is necessary to obtain accurate compression flow data, in the present work neither lubrication nor Rastegaev-type samples were utilized. This is because the aim of the this study was not to obtain accurate flow curves of S235JR, but to evaluate different acquisition approaches. For the same reason, neither barreling nor temperature corrections were applied.

As regards data monitoring, two techniques were utilized to acquire load and displacement experimental data. For the measurement of the kinematics of the upper die, a Photron Fastcam-APX RS250K high-speed camera with appropriated illumination lamps was used (Fig. 2). This camera offers recording rates up to 250,000 fps. In this study experimental measurements were taken at 15,000 fps. Random point-patterns

were generated in the upper (moving) and lower (static) dies, and the deformation kinematics were obtained with the DIC software GOM Correlate, (Fig. 3). For safety reasons, the deformation of the sample was carried out inside a cavity located in the lower side of the upper die. Therefore, for the strain calculation of the sample, the linear displacement of the upper die was taken into account. The upper die was considered as rigid; and consequently the motion of the upper die was determined to be equal to the deformation kinematics of the sample. To acquire the impact force, a piezoelectric load cell connected to an oscilloscope was employed (Fig. 2). This force sensor was mounted directly inside the lower static die of the hammer, and the acquisition frequency was 300 kHz.

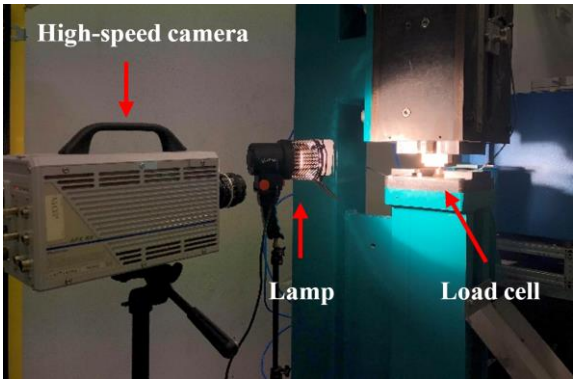

Fig. 2. Data acquisition set-up.

3. Results and discussion

In this section, the experimental results are presented. First of all, reference flow curves are discussed, which were generated combining the kinematics obtained by the high-speed camera and the force measured by the load cell. Next, the two analytically calculated flow curves are presented, one using the data obtained by the high-speed camera, and the other the data acquired by the force sensor. Finally, the flow curves generated by the three acquisition approaches are compared.

Henceforth, the lowest tested strain rate (150 s^{-1}) is referred to as case 1, the strain rate of 200 s^{-1} as case 2, the next higher strain rate (235 s^{-1}) as case 3, and the highest tested strain rate (260 s^{-1}) as case 4. Three repetitions were performed for each of the four velocities and a very low deviation was observed in all cases. Mean values were calculated for each case. As the test was automated, this undoubtedly enhanced the repeatability of the results.

3.1. Reference curves

Reference flow curves were generated by combining the motion data obtained from the high-speed camera and the force measured by the load cell. As for the high-speed camera results, Fig. 4 shows the DIC technique employed for the acquisition of the kinematics of the upper and lower dies. A mean value of all the measured points was calculated in each of the dies. The displacement and velocity data of the four tested strain rates is presented in Fig. 5. As expected, it is observed that the higher the impact speed, the greater the sample deformation. A velocity peak can be seen at the beginning of each speed-curve, at the instant in which the upper die makes contact with the sample. This is likely due to the lack of lubrication between both surfaces, and thus the use of lubrication may smooth those peaks. It is also observed that the speed curves follow a relatively linear tendency.

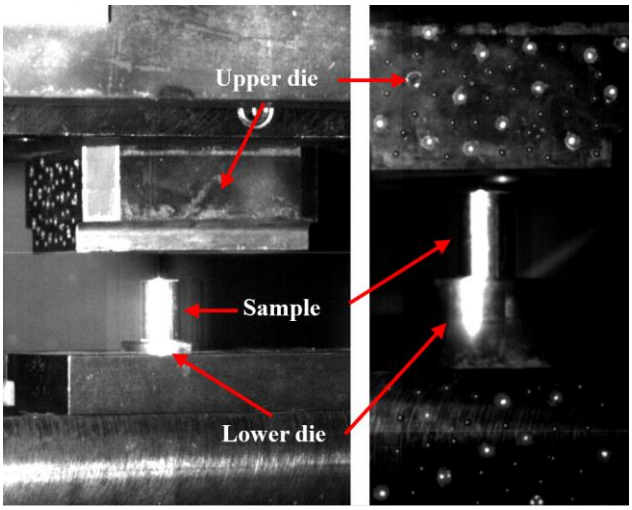

Fig. 3. Upper moving and lower static dies recorded with Photron Fastcam-APX RS250K high-speed camera.

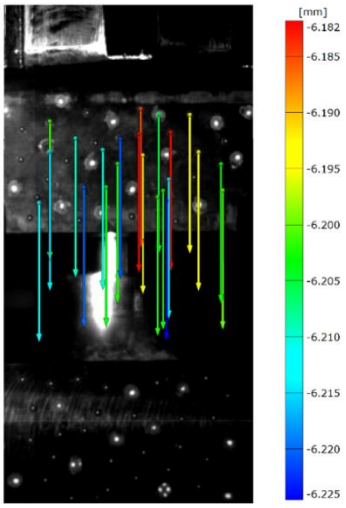

Fig. 4. Displacement of the upper die calculated with GOM Correlate DIC software.

It is important to highlight that only the motion data of the upper die was employed to generate the flow curves, disregarding the displacement of the lower die. In the most unfavorable case, that of the highest velocity, the maximum displacement of the lower die was of 0.32 mm while the maximum displacement of the upper die was 11.67 mm. In this case, the displacement of the lower die is 2.74 % of the displacement of the upper die. Fig. 6 shows the acceleration of the upper die during the high-speed deformation. Although the tendency is similar from case to case, high levels of noise and significant variations in acceleration values can be observed.

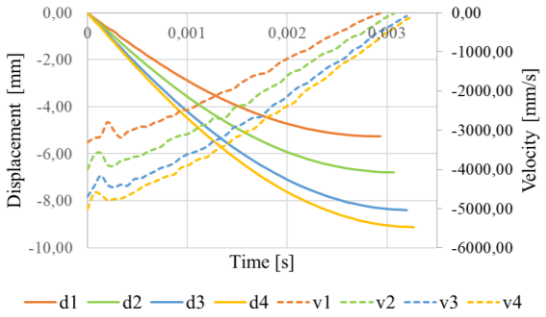

Fig. 5. Displacement and velocity of the upper die acquired with high-speed camera.

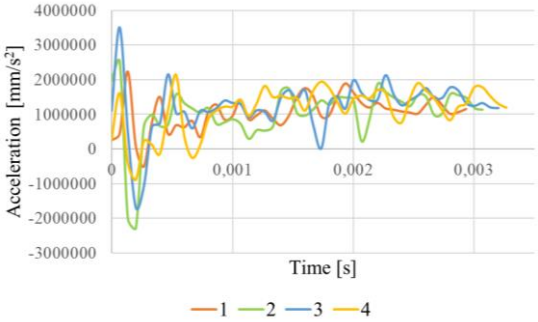

Fig. 6. Acceleration of the upper die acquired with high-speed camera.

True strain values were calculated taking into account the displacement of the upper die measured by the high-speed camera (Eq. 2). Once true strain was calculated, true strain rate values were also obtained (Eq. 1). With respect to the evolution of strain rates during the uniaxial upsetting tests, once the upper die comes into contact with the sample, the die starts decelerating with a linear trend (Fig. 5). Fig. 7 shows that the strain rate remains relatively constant up to a certain strain level, and this strain level is higher in the case of the highest deformation speed. Taking this into account, if a constant strain rate is sought, a criterion is needed to specify the strain level until which the test can be considered as strain-rate-constant. In the case of this work, a constant strain rate was considered until the strain rate dropped below 90 % of the initial strain rate value. The constant strain rate ranges are marked as solid lines in Fig. 7 and the non-constant ranges as dotted lines. The figure shows that at the highest speed, strain rates of 250 s^{-1} are reached. In industrial hammer processes strain rates of up to 200 $s^{-1}$are attained, and thus the tests performed with the instrumented forging hammer covered the range of strain rates found in industry.

As for data obtained by the load cell, Fig. 8 shows the force acquisition during the compression tests. It can be seen that the higher the strain rate, the higher the force needed to deform the material. As in the case of

the velocities acquired by the high-speed camera, a peak is observed at the beginning of the force curves. This can be attributed to the first contact between the upper die and the sample, and could be smoothed by applying lubrication between both surfaces.

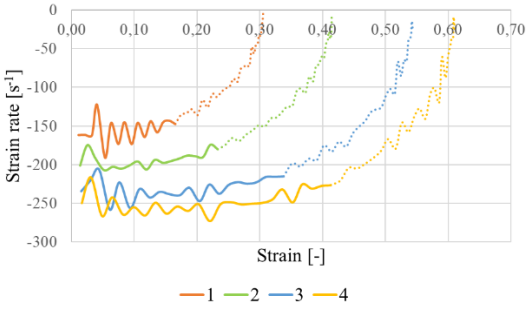

Fig. 7. Strain rates acquired with high-speed camera.

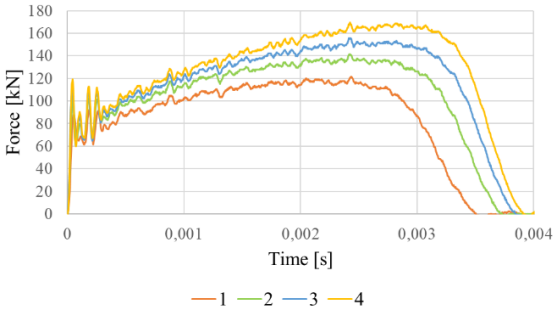

Fig. 8. Force data acquired with load cell.

Fig. 9 sets out force vs displacement curves generated by combining the displacement captured with the high-speed camera, and the force acquired with the load cell. Additionally, a force vs displacement curve obtained from a quasi-static compression test performed in a universal electro-mechanic drive Instron-4206 testing machine is shown. Compression tests in this standard testing machine were performed at a strain rate of 0,001 s^{-1}, significantly lower than the strain rates of the instrumented forging hammer, hence the difference in force.

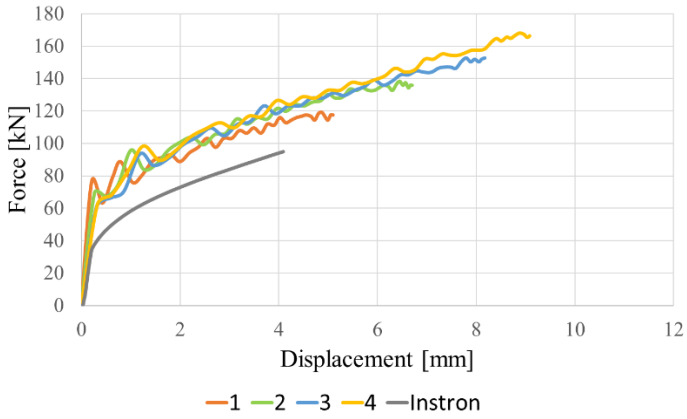

Fig. 9. Reference force vs displacement data.

To generate a typical stress-strain curve, displacement values were converted into true strain values by Eq. 2, and force values were converted into stress values using Eq. 3:

$$\varepsilon = \ln\left(\frac{h}{h_0}\right) \tag{2}$$

$$\sigma = \frac{\vec{F}}{A} \tag{3}$$

where h is the height of the sample at each point of the test, h_0 is the initial height; and F and A are the force and transversal area at each point of the test, respectively. The instantaneous transversal area of the sample was calculated based on the following assumption (Eq. 5):

$$V_0 = V \tag{4}$$

$$A = \frac{A_0 \cdot h_0}{h} \tag{5}$$

where A_0 and h_0 are the initial area and initial height of the sample, respectively, and h is the instantaneous height of the sample measured by the high-speed camera. In cases of considerable barreling, this assumption can lead to errors. Little barreling was observed in the uniaxial upsetting tests performed in the current work, and therefore the assumption can be considered as valid (Fig. 10).

Fig. 10. Tested samples at four different strain rates

Reference true stress vs true strain flow curves are presented in Fig. 11. Interestingly, a maximum valid true strain of 0.42 was achieved at the highest strain rate. Intermediate strain rate flow curves show some noise which could be mathematically smoothed if needed. Quasi-static tensile and compression curves of tests performed in the aforementioned universal Instron testing machine are included in the figure as a reference.

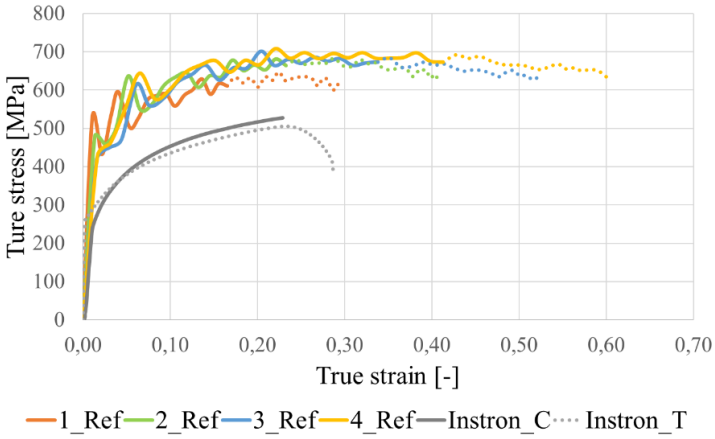

Fig. 11. Reference medium strain rate flow curves, and Intron compression (C) and Instron tensile (T) curves

3.2. Curves from high-speed camera data only

Once the reference flow curves were obtained by combining high-speed camera data and load cell data, a second approach was used to evaluate its ability to calculate valid flow data under hammer forging conditions. For this second approach stress vs strain curves were generated by employing only data acquired by the high-speed camera. As the kinematics of the upper and lower dies can be directly acquired by the high-speed camera, the true strain is obtained. To analytically calculate the force data from the motion data measured by the high-speed camera, Newton's second law was followed (Eq. 6):

$$\vec{F} = m \cdot \vec{a} \tag{6}$$

where m is the total mass of the moving elements and $\vec{a}$ is the acceleration acquired by the camera. The mass of all the moving elements in the upper die was measured at 92 kg. As an example, in case 3 force acquired by the load cell and the force analytically calculated from camera data is shown in Fig. 12. Although the calculated curve follows the tendency of the reference load cell data, significant noise and a

lack of sharpness can be distinguished. Moreover, at the beginning of the curve, at small strains, the calculated curve does not represent the reference curve.

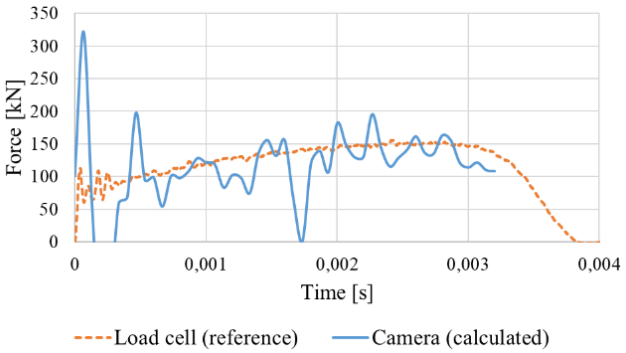

Fig. 12. Load cell (reference) force vs camera (calculated) force for the case 3.

By analytically calculating the force in all the cases (Eq. 6), and converting it into stress (Eq. 3), stress vs strain curves were generated from only the high-speed camera data (Fig. 13). Each case is presented separately as the noise makes differentiation difficult. Although the calculated flow curves follow the reference force tendencies measured by the load cell, significant noise is discernable in all cases. In addition, this monitoring technique is unable to represent the beginning of the flow curve at small strains.

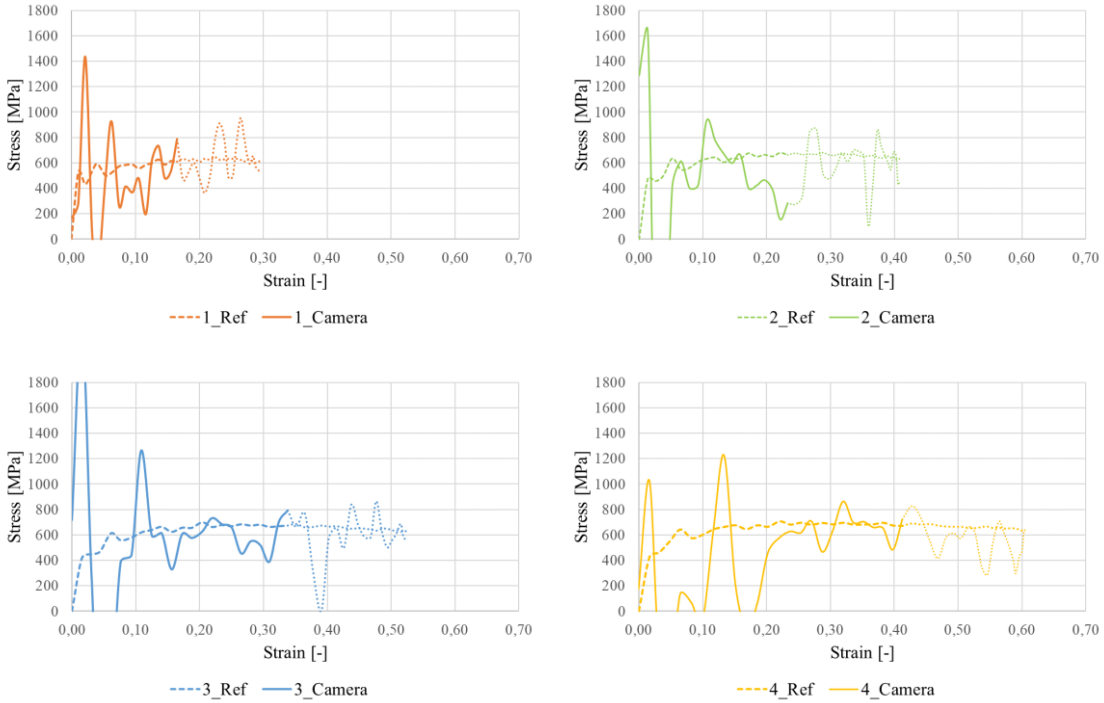

Fig. 13. Reference flow curves vs calculated (camera) flow curves for all tested velocities.

3.3. Curves from load cell data only

Finally, a third acquisition approach was analyzed, in which medium strain rate flow curves were generated by only employing data acquired by the load cell. Deformation forces were directly acquired by the load cell, and to extract strain and stress data, acceleration was first calculated with Newton's second law (Eq. 7):

$$\vec{a} = \frac{\vec{F}}{m} \tag{7}$$

where *m* is the total mass of the moving elements and $\vec{F}$ is the force acquired by the load cell directly. It was known that the mass of all moving elements was 92 kg. Taking case 3 as an example, acceleration acquired by the high-speed camera and acceleration analytically calculated from load cell data is presented in Fig. 14. It can be clearly seen that the calculated acceleration follows the reference tendency. Furthermore, the calculated acceleration signal is significantly smoother and sharper than the acceleration acquired by the high-speed camera.

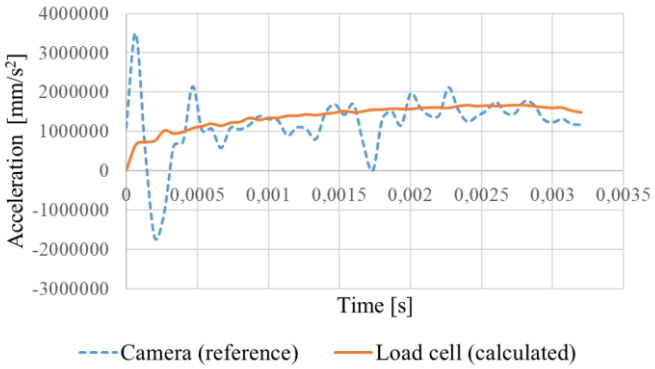

Fig. 14. Camera (reference) acceleration vs load cell (calculated) acceleration for the case 3.

Once the acceleration was calculated, the equation of an accelerated linear motion was employed to calculate the position of the upper die at each point of the test (Eq. 6):

$$\vec{s} = \vec{s}_0 + \vec{v}_0 \cdot t + \frac{1}{2} \cdot \vec{a} \cdot t^2 \tag{6}$$

where $\vec{s}_0$ is the initial position of the upper die, $\vec{v}_0$ is its initial velocity, $\vec{a}$ is its acceleration, and *t* is the time. To calculate position data using this equation, the initial velocity is the only variable that cannot be measured or analytically calculated from load-cell data. Thus, in this case the velocity of the upper die just before the impact measured by the high-speed camera was used. However, as a future line, to analytically calculate the displacement of the upper die without employing an expensive and complex high-speed camera, the idea is to equip the hammer with a simple velocity measuring setup. To do so, two electrical switches separated by a known distance and connected to the same oscilloscope of the load cell will be utilized. The two switches will detect the upper die just before impact. Knowing the time difference between the two detectors and the distance between the two switches, the velocity of the upper die just before the impact will be calculated by Eq. 7:

$$\vec{v} = \frac{d}{\Delta t} \tag{7}$$

were *d* and Δt is the distance between the two detectors and the time difference between the two detections, respectively. By calculating the displacement in all cases (Eq. 6) and converting it into stress and strain data (Eq. 2, 3), flow curves were generated utilizing only the load cell data (Fig. 15).

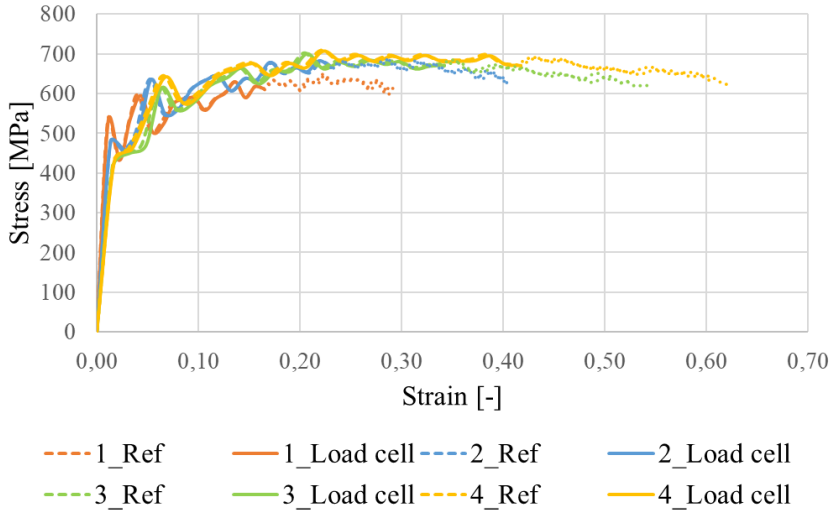

Fig. 15. Reference flow curves vs calculated (load cell) flow curves for all tested velocities.

The analytically calculated flow curves utilizing solely data acquired by the load cell and the reference flow curves show very good agreement. Similar noise is discernable in both cases and the deviation between them is minimum.

4. Conclusions

In this study, a novel automatic forging simulator comprised of an instrumented forging hammer capable of performing intermediate speed deformations is presented. Three data acquisition approaches were evaluated, so as to select the most appropriate to obtain valid rheological data from intermediate strain rate upsetting tests. The main conclusions are set out below:

- Flow data calculated by employing only the high-speed camera was not sufficiently accurate and significant noise was discernable in all cases.
- Although analytically calculated forces followed reference force tendencies measured by the load cell, this monitoring approach was not sharp enough to precisely represent the beginning of the curve at small strain values.
- Stress vs strain data calculated by only employing data acquired by the load cell showed very good agreement with the reference flow curves without the need for an expensive and complex high-speed camera. Similar noise is discernable in both cases and the deviation between them is minimum. Moreover, no time consuming DIC post-processing was required, and thus the flow data calculation is considerably faster.
- Based on these conclusions, it was determined that this acquisition approach will be implemented in the instrumented forging hammer, for future material behavior analysis at medium strain rates.

Acknowledgements

This work was funded by the Basque Government through the OGForge (Piezas forjadas de prestaciones extremas para el sector Oil & Gas mediante procesos de forja eficientes optimizados por modelos complejos de evolución microstructural), and DIGICUT (Estudio fundamental de procesos de corte y definición de las bases para su digitalización) research projects. The authors would also like to thank ULMA Forja S.Coop. and Fagor Arrasate S.Coop. for their economic and technical support.

References

[1] Altan T, Ngaile G. ASM Cold and Hot Forging. 2005.

[2] Bhujangrao T, Froustey C, Iriondo E, Veiga F, Darnis P, Mata FG. Review of intermediate strain rate testing devices. Metals (Basel) 2020;10:1–24. https://doi.org/10.3390/met10070894.

[3] Prasad YVRK, Rao KP, Sasidhara S. Hot Working Guide - A Compendium of Processing Maps. 2nd ed. 2015. https://doi.org/10.1016/B978-0-08-033454-7.50019-X.

[4] YE X jue, GONG X juan, YANG B biao, LI Y ping, NIE Y. Deformation inhomogeneity due to sample–anvil friction in cylindrical compression test. Trans Nonferrous Met Soc China (English Ed 2019;29:279–86. https://doi.org/10.1016/S1003-6326(19)64937-X.

[5] Torrente G. Numerical and experimental studies of compression-tested copper: Proposal for a new friction correction. Mater Res 2018;21. https://doi.org/10.1590/1980-5373-mr-2017-0905.